Acta Crystallographica Section F
Structural Biology and Crystallization Communications
ISSN 1744-3091

Structure of *Mycobacterium tuberculosis* phosphopantetheine adenylyltransferase in complex with the feedback inhibitor CoA reveals only one active-site conformation

T. Wubben[a] and A. D. Mesecar[b]*

[a]Department of Biochemistry and Molecular Genetics, University of Illinois at Chicago, Chicago, Illinois, USA, and [b]Departments of Biological Sciences and Chemistry, Purdue University, West Lafayette, Indiana, USA

Correspondence e-mail: amesecar@purdue.edu

Received 11 January 2011
Accepted 23 March 2011

PDB Reference: PPAT–CoA complex, 3pnb.

Phosphopantetheine adenylyltransferase (PPAT) catalyzes the penultimate step in the coenzyme A (CoA) biosynthetic pathway, reversibly transferring an adenylyl group from ATP to 4′-phosphopantetheine to form dephospho-coenzyme A (dPCoA). To complement recent biochemical and structural studies on *Mycobacterium tuberculosis* PPAT (*Mt*PPAT) and to provide further insight into the feedback regulation of *Mt*PPAT by CoA, the X-ray crystal structure of the *Mt*PPAT enzyme in complex with CoA was determined to 2.11 Å resolution. Unlike previous X-ray crystal structures of PPAT–CoA complexes from other bacteria, which showed two distinct CoA conformations bound to the active site, only one conformation of CoA is observed in the *Mt*PPAT–CoA complex.

1. Introduction

In bacteria, CoA is synthesized from pantothenate in five enzymatic steps common to all organisms, but the source of the pantothenate differs (Genschel, 2004). Some bacteria are capable of *de novo* pantothenate production while others possess the capability of utilizing extracellular pantetheine for CoA biosynthesis, but virtually all bacteria also have mechanisms to uptake extracellular pantothenate (Jackowski & Rock, 1984; Gerdes *et al.*, 2002). These three pathways converge at the penultimate step in the pathway catalyzed by phosphopantetheine adenylyltransferase (PPAT), which reversibly transfers an adenylyl moiety from ATP to 4′-phosphopantetheine (PhP) to produce dephospho-CoA (dPCoA) and pyrophosphate (PP_i). The PPAT-catalyzed reaction has been proposed and subsequently confirmed to be a secondary rate-limiting step within the CoA-biosynthetic pathway that is negatively regulated by CoA (Jackowski & Rock, 1981, 1984; Rock *et al.*, 2003; Miller *et al.*, 2007). With all flux of the CoA-biosynthetic pathway funneling through PPAT, the regulatory character of this enzyme may prove vital to its potential as an antibiotic target.

To date, a number of X-ray crystal structures of PPAT orthologs have been determined [PDB entries 1b6t (Izard & Geerlof, 1999), 1qjc (Izard, 2002), 1gn8 (Izard, 2002), 1h1t (Izard, 2003), 1od6 (Takahashi *et al.*, 2004), 1tfu (Morris & Izard, 2004), 3f3m (Lee *et al.*, 2009), 3nba, 3nbk (Wubben & Mesecar, 2010), 3k9w (Edwards *et al.*, 2011), 3l92 and 3l93 (J. Osipiuk, N. Maltseva, M. Makowska-grzyska, K. Kwon, W. F. Anderson & A. Joachimiak, unpublished work). However, detailed biochemical and kinetic studies on PPAT for the majority of these bacterial species are lacking, with the exceptions of *Escherichia coli* and *Mycobacterium tuberculosis* PPAT. Recently, we performed a detailed kinetic, thermodynamic and structural study on PPAT from *M. tuberculosis* (*Mt*PPAT) and observed cooperativity in its binding of substrates and products (Wubben & Mesecar, 2010). To complement these findings and to provide further insight into the regulatory character of *Mt*PPAT and how it may differ from that of other bacterial species, the X-ray crystal structure of the *Mt*PPAT–CoA complex is presented here.

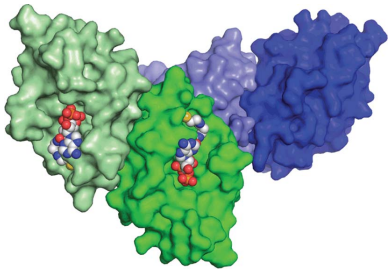

Table 1
Data-collection and refinement statistics.

Values in parentheses are for the last resolution shell.

Data collection	
Space group	*P*321
Unit-cell parameters (Å, °)	$a = b = 114.5$, $c = 134.5$, $\alpha = \beta = 90.0$, $\gamma = 120.0$
Resolution (Å)	50.00–2.11
No. of observed reflections	636565
No. of unique reflections	53413
$R_{\rm merge}$ (%)	10.7 (54.7)
$\langle I/\sigma(I)\rangle$	26.0 (3.9)
Completeness (%)	95.0 (92.7)
Refinement	
Resolution range	50.00–2.11 (2.16–2.11)
No. of reflections in working set	50586 (3820)
No. of reflections in test set	2827
$R_{\rm work}$ (%)	21.5
$R_{\rm free}$ (%)	24.8
Average structure *B* factor (Å^2)	25.0
Average ligand *B* factor (Å^2)	50.6†
R.m.s. deviations	
Bond lengths (Å)	0.01
Bond angles (°)	1.00
Ramachandran plot	
Favored (%)	98.5
Outliers (%)	0.2

† Average determined from all four bound ligands in the asymmetric unit.

2. Materials and methods

2.1. Protein expression, purification and crystallization

The cloning, expression and purification of *Mt*PPAT have been described elsewhere (Wubben & Mesecar, 2010). Using the hanging-drop vapor-diffusion method, cocrystals of the *Mt*PPAT–CoA complex appeared overnight at 298 K after mixing 2 µl of a solution consisting of 10 mg ml^{-1} *Mt*PPAT, 5 m*M* $MgCl_2$ and 5 m*M* CoA in 20 m*M* Tris pH 8, 150 m*M* NaCl and 1 m*M* DTT (dithiothreitol) with 2 µl precipitant solution that consisted of 0.1 *M* Tris base pH 8.0 and 0.15 *M* magnesium formate.

2.2. Data collection and structure determination

Single crystals of the *Mt*PPAT–CoA complex were transferred to nylon loops and then submerged in cryoprotectant solution consisting of the precipitant solution described above supplemented with 30%(*v*/*v*) glycerol, 5 m*M* $MgCl_2$ and 5 m*M* CoA. The crystals were subsequently flash-frozen in liquid nitrogen. X-ray data for the co-crystal complex were collected on the Life Sciences Collaborative Access Team (LS-CAT) 21-ID-G beamline at the Advanced Photon Source, Argonne National Laboratory. X-ray diffraction data were processed and scaled using *HKL*-2000 (HKL Research, Charlottesville, Virginia, USA; Otwinowski & Minor, 1997). Data-processing and refinement statistics are summarized in Table 1.

Since trigonal space groups are prone to twinning (Wu *et al.*, 2005; Fernández-Millán *et al.*, 2008), the diffraction data were analyzed using the *TRUNCATE* program in the *CCP*4 suite (Winn *et al.*, 2011). The analysis indicated a twinning operator of $h + k$, $-k$, $-l$ and the *H*-test suggested a twinning fraction of 16% (Yeates, 1988). Likewise, the *L*-test (Padilla & Yeates, 2003) suggested that the data were twinned: $|L| = 0.436$ (untwinned, 0.5; perfect twin, 0.375). In addition, the mean value of the second moment of intensity was 1.864; the expected values are 1.5 for a perfect twin and 2.0 for an untwinned crystal (Yeates, 1997). Pseudo-translation was not detected. Upon application of the *DETWIN* program in the *CCP*4 suite (Winn *et al.*, 2011), the twinning fraction decreased to 8% as per the *H*-test, $|L|$ increased to 0.454 and the second moment of intensities of the acentric reflections increased to 2.098, indicating that very little twinning remained.

Using the detwinned data, the *Mt*PPAT–CoA structure was solved *via* molecular replacement using the program *Phaser* (Read, 2001) with a single-monomer model from the apo *Mt*PPAT–PhP structure (PDB code 3nbk; Wubben & Mesecar, 2010) as a search model. The structure was refined using *REFMAC* in the *CCP*4 suite and *WinCoot* was used for model building (Winn *et al.*, 2011). Water molecules were added to $F_o - F_c$ density peaks that were $\geq 3.0\sigma$ using the 'Find Waters' function in the *WinCoot* program. The quality of the final model was validated by the *SFCHECK* function of the *CCP*4 suite and by *MolProbity* (Chen *et al.*, 2010).

3. Results and discussion

3.1. X-ray structure of *Mt*PPAT–CoA complex

The crystal structure of the *Mt*PPAT–CoA complex was solved in space group *P*321 to 2.11 Å resolution. The asymmetric unit contains four protomers: two belong to one biologically significant hexamer and the other two belong to an adjacent hexamer in the crystal, with the two protomers from each hexamer arranged across the dyad axis (Fig. 1*a*). Each protomer within the asymmetric unit contains a single CoA molecule in the active site. The CoA molecules refine with full occupancy to an average *B* factor of 50.6 Å^2 (the average is for all four CoA molecules in the asymmetric unit), with the mean *B* factor of the overall structure refining to 25.0 Å^2 (Fig. 1*b*). The pantetheine moiety of the CoA molecule binds within the *Mt*PPAT active site in a similar fashion to that observed for the substrate PhP (Wubben & Mesecar, 2010; Fig. 2*a*) as well as that of PhP in complex with *Thermus thermophilus* PPAT (PDB code 1od6; Takahashi *et al.*, 2004). However, as judged from final $F_o - F_c$ and $2F_o - F_c$ electron-density maps associated with CoA within the active site (Fig. 1*b*), the adenylate moiety of CoA exhibits a greater degree of disorder than the pantetheine portion of CoA. This disorder is likely to occur because the adenine group is not anchored as tightly within the adenyl binding pocket compared with the ATP substrate analog adenosine-5′-[(α,β)-methyleno]triphosphate (AMPcPP; PDB code 3nba; Wubben & Mesecar, 2010; Fig. 2*a*). Instead, the adenine group of CoA projects into the solvent channel of the biologically significant hexamer (Fig. 2*b*) and is in loose contact with the enzyme through direct hydrogen bonds to the side chains of Asp94 and Ser128 (Fig. 1*b*).

3.2. Comparison of PPAT–CoA complexes from different organisms

The X-ray crystal structures of two other PPAT orthologs in complex with CoA, *E. coli* PPAT–CoA (PDB entry 1h1t; Izard, 2003) and *Yersinia pestis* PPAT–CoA (PDB code 3l92; unpublished work), have also been determined. *E. coli* PPAT (*Ec*PPAT) and *Y. pestis* PPAT (*Yp*PPAT) both exhibit two different CoA-binding modes, whereas *Mt*PPAT exhibits only a single binding mode (Fig. 3). In the *Ec*PPAT–CoA crystal complex the different binding modes of CoA are observed in the two different subunits (*A* and *B*) of the asymmetric unit, whereas in the *Yp*PPAT structure the different binding modes are observed within the same active site of the single protomer in the asymmetric unit with occupancy values of 0.4 and 0.6. The conformation of CoA bound to *Mt*PPAT, as detailed above, is similar to the conformation of CoA bound to subunit *B* of *Ec*PPAT (Izard, 2003) and *Yp*PPAT. In the alternate binding mode, which is shared between subunit *A* of *Ec*PPAT and *Yp*PPAT, the pantetheine arm of CoA is bent in the opposite direction (Izard, 2003). The dual *versus* single binding modes may result from the steric hindrance imposed by

residues 71–74 in the crystal structures of *Ec*PPAT and *Yp*PPAT (Izard, 2003). The overall root-mean-square deviations (r.m.s.d.s) between subunits *A* and *B* of *Ec*PPAT and subunit *A* of *Mt*PPAT are 1.11 and 1.13 Å, respectively. Likewise, the overall r.m.s.d. between *Yp*PPAT and subunit *A* of *Mt*PPAT is 1.29 Å. One region in these structural comparisons in which structural differences are observed is residues 71–74. Conversely, when examining the overall r.m.s.d. between the orthologs that exhibit dual CoA-binding modes, specifically the respective subunits (*A* and *B*) of *Ec*PPAT and *Yp*PPAT, residues 71–74 did not deviate much, suggesting that this region may be responsible for the dual binding mode. Therefore, the steric hindrance exerted by these residues on the CoA molecule in *Ec*PPAT and *Yp*PPAT may not be present to the same degree in *Mt*PPAT, allowing CoA to bind to each protomer in a similar manner.

While it is tempting to speculate that the different binding modes of CoA observed in the *Ec*PPAT structure represent the two independent binding sites determined *via* isothermal titration calorimetry (ITC; Miller *et al.*, 2007), the ITC experiments were performed at pH 8 whereas the X-ray structure was determined at pH 5. The binding affinity of CoA for *Ec*PPAT has been shown to be pH-dependent (Geerlof *et al.*, 1999; Miller *et al.*, 2007). Furthermore, biochemical characterization of *Yp*PPAT has not yet been reported, so interpretation or rationalization of its dual CoA-binding modes cannot be ascertained. However, by solving the X-ray crystal structure of the *Mt*PPAT–CoA complex at pH 8.0 a direct comparison can be made with the thermodynamic binding profile of CoA, which was also determined at pH 8.0 (Wubben & Mesecar, 2010). The interaction of CoA with *Mt*PPAT, as examined by ITC, was observed to be sequential in nature, suggesting that the transition to each ligation state is not identical and an asymmetric quarternary structure forms in solution upon the binding of CoA to each respective site on the hexamer. Similar changes between ligation states have also been

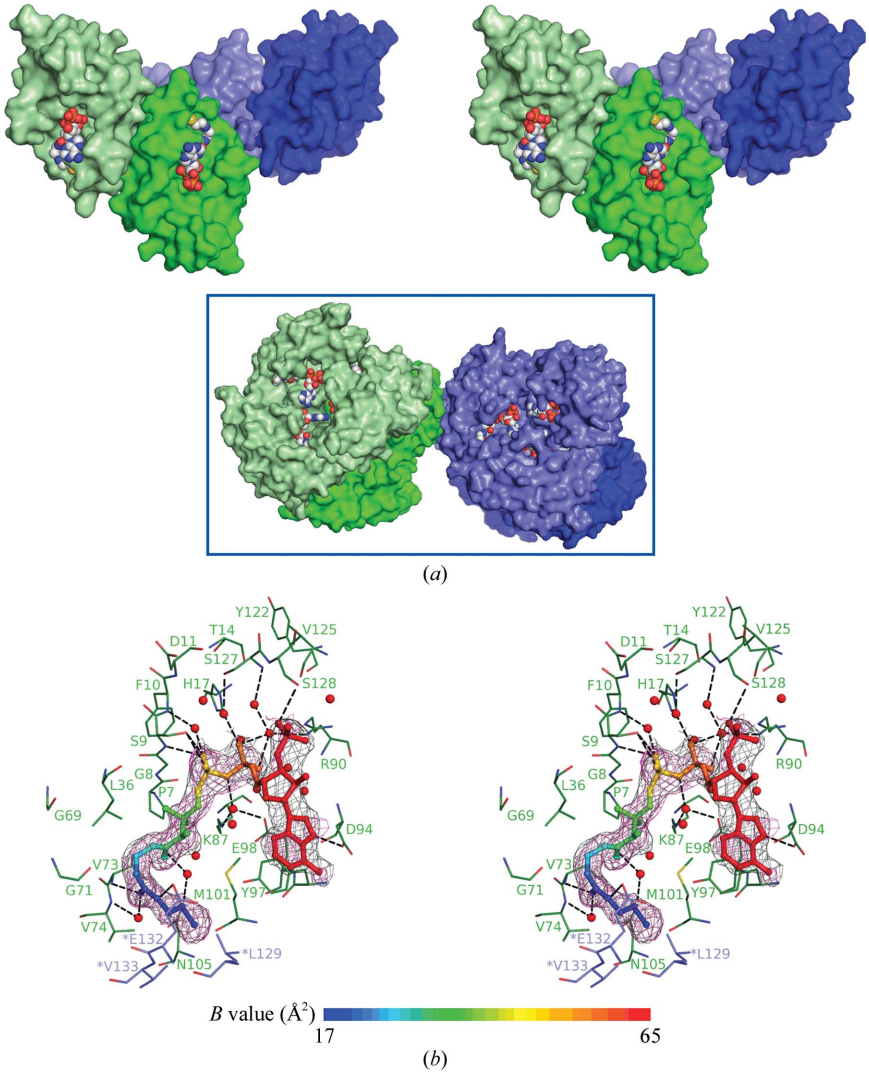

Figure 1
*Mt*PPAT in complex with CoA. (*a*) Wall-eyed stereoview of the asymmetric unit of the *Mt*PPAT–CoA crystal complex. Two protomers belong to one hexamer (shades of green) and the other two belong to an adjacent hexamer (shades of blue) in the crystal (inset). The two protomers from each respective hexamer are arranged across the dyad axis. The protomers are shown in surface representation. CoA is bound to all four protomers in the asymmetric unit and is depicted in space-filling representation. C atoms are shown in gray, N atoms in blue, S atoms in yellow, O atoms in red and phosphates in orange. (*b*) Wall-eyed stereoview of the amino-acid residues and water molecules in contact with CoA in the active site of *Mt*PPAT. Subunit *A* of *Mt*PPAT is colored forest green. Residues from the adjacent subunit across the trimer threefold axis are shown in slate and marked with an asterisk. Hydrogen bonds are depicted as dashed lines and water molecules are depicted as red spheres. CoA is colored according to the *B* factor of each atom and the $F_o - F_c$ electron density (light magenta) of CoA is contoured at 2.5σ, while the $2F_o - F_c$ electron density (gray) is contoured at 1.0σ. The mean *B* factor of the protein is 25.0 Å^2, whereas the mean *B* factor of all four CoA molecules in the asymmetric unit is 50.6 Å^2 (49.2 Å^2 for the CoA molecule in subunit *A*). The mean *B* factor of CoA is greater than that of the protein, mainly owing to the disorder of the CoA adenylate moiety.

observed in inosine monophosphate dehydrogenase and support conformational differences at each of the sites (Bruzzese & Connelly, 1997). The crystal structure of the *Mt*PPAT–CoA complex lends some support to this binding model since multiple protomers of CoA are observed in the asymmetric unit despite the fact that only a single major binding mode or conformation of CoA is observed. The binding of CoA to one protomer may therefore result in a cascade of small conformational changes that ultimately result in the binding of CoA to six binding sites of the hexamer, with each site being thermodynamically non-equivalent during the sequential binding process. The differences in the CoA-binding sites and the CoA-binding modes between the different PPAT orthologs may suggest variation in the ability of CoA to regulate the respective enzymes in a feedback method.

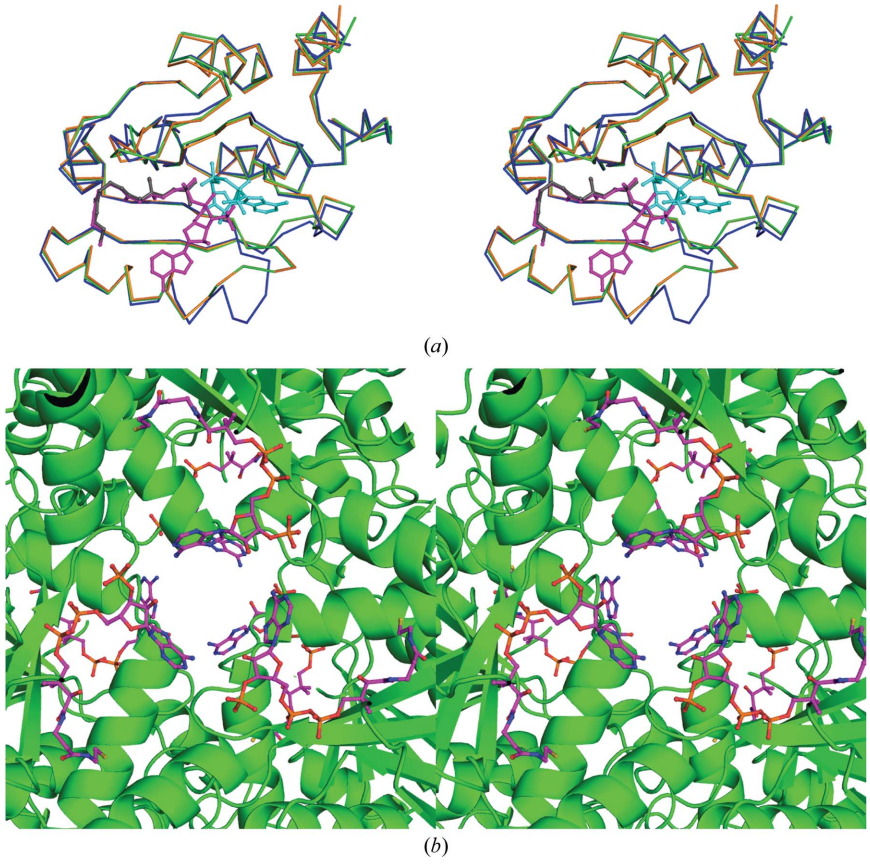

Figure 2
Relationship between the different modes of ligand binding to *Mt*PPAT. (*a*) Superposition of different ligand-complexed forms of *Mt*PPAT. Subunit *A* of *Mt*PPAT–CoA is shown in green, *Mt*PPAT–PhP is shown in orange (PDB code 3nbk, subunit *A*; Wubben & Mesecar, 2010) and *Mt*PPAT–AMPcPP is shown in blue (PDB code 3nba, subunit *C*; Wubben & Mesecar, 2010). CoA (magenta), PhP (gray) and AMPcPP (cyan) are shown in ball-and-stick representation. (*b*) Projection of the adenylate moiety of CoA into the solvent channel of the biologically significant hexamer of *Mt*PPAT. The view is down the triad axis of the hexamer. *Mt*PPAT (green) is depicted in cartoon representation, with CoA shown in ball-and-stick representation.

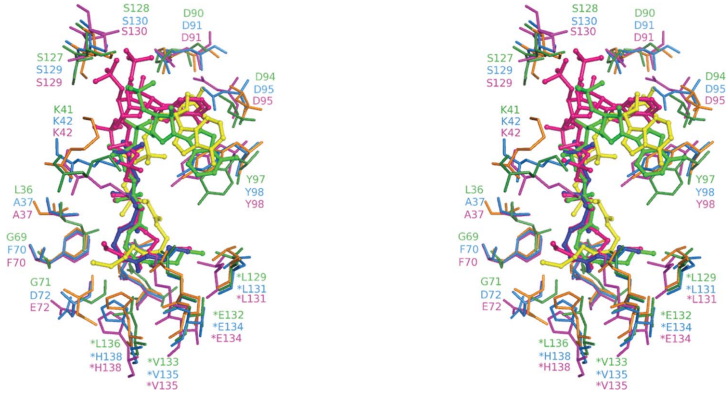

Figure 3
Comparison of the CoA-binding mode in PPAT from different organisms. *Y. pestis* PPAT–CoA (PDB code 3l92, magenta; unpublished work), *E. coli* PPAT–CoA subunit *A* (PDB code 1h1t, orange; Izard, 2003) and *E. coli* PPAT–CoA subunit *B* (PDB code 1h1t, blue; Izard, 2003) are superimposed onto *Mt*PPAT–CoA (subunit *A*, forest green). CoA bound to *Y. pestis* PPAT is shown in hot pink, CoA bound to *E. coli* PPAT is shown in yellow (subunit *A*) and blue (subunit *B*) and CoA bound to *Mt*PPAT is shown in green. Residues from *Mt*PPAT, *E. coli* PPAT subunit *B* and *Y. pestis* PPAT that are marked with an asterisk are from the adjacent subunit across the triad axis. Residues from subunit *A* of *E. coli* PPAT were not labeled because they are the same as those labeled from subunit *B*.

We thank the beamline staff at the Life Sciences Collaborative Access Team (LS-CAT) 21-ID-G beamline at the Advanced Photon Source, Argonne National Laboratory. This research was supported by NIH Pharmacological Sciences Training Grant 1T32 GM010388-05 and by a grant (AI056575) from the National Institutes of Health.

References

Bruzzese, F. J. & Connelly, P. R. (1997). *Biochemistry*, **36**, 10428–10438.
Chen, V. B., Arendall, W. B., Headd, J. J., Keedy, D. A., Immormino, R. M., Kapral, G. J., Murray, L. W., Richardson, J. S. & Richardson, D. C. (2010). *Acta Cryst.* D**66**, 12–21.
Edwards, T. E., Leibly, D. J., Bhandari, J., Statnekov, J. B., Phan, I., Dieterich, S. H., Abendroth, J., Staker, B. L., Van Voorhis, W. C., Myler, P. J. & Stewart, L. J. (2011). *Acta Cryst.* F**67**, doi:10.1107/S1744309111004349.
Fernández-Millán, P., Kortazar, D., Lucas, M., Martínez-Chantar, M. L., Astigarraga, E., Fernández, J. A., Sabas, O., Albert, A., Mato, J. M. & Martínez-Cruz, L. A. (2008). *Acta Cryst.* F**64**, 605–609.
Geerlof, A., Lewendon, A. & Shaw, W. V. (1999). *J. Biol. Chem.* **274**, 27105–27111.
Genschel, U. (2004). *Mol. Biol. Evol.* **21**, 1242–1251.
Gerdes, S. Y. *et al.* (2002). *J. Bacteriol.* **184**, 4555–4572.
Izard, T. (2002). *J. Mol. Biol.* **315**, 487–495.
Izard, T. (2003). *J. Bacteriol.* **185**, 4074–4080.
Izard, T. & Geerlof, A. (1999). *EMBO J.* **18**, 2021–2030.
Jackowski, S. & Rock, C. O. (1981). *J. Bacteriol.* **148**, 926–932.
Jackowski, S. & Rock, C. O. (1984). *J. Bacteriol.* **158**, 115–120.
Lee, H. H., Yoon, H.-J., Kang, J. Y., Park, J. H., Kim, D. J., Choi, K.-H., Lee, S.-K., Song, J., Kim, H.-J. & Suh, S. W. (2009). *Acta Cryst.* F**65**, 987–991.
Miller, J. R., Ohren, J., Sarver, R. W., Mueller, W. T., de Dreu, P., Case, H. & Thanabal, V. (2007). *J. Bacteriol.* **189**, 8196–8205.
Morris, V. K. & Izard, T. (2004). *Protein Sci.* **13**, 2547–2552.
Otwinowski, Z. & Minor, W. (1997). *Methods Enzymol.* **276**, 307–326.
Padilla, J. E. & Yeates, T. O. (2003). *Acta Cryst.* D**59**, 1124–1130.
Read, R. J. (2001). *Acta Cryst.* D**57**, 1373–1382.
Rock, C. O., Park, H. W. & Jackowski, S. (2003). *J. Bacteriol.* **185**, 3410–3415.
Takahashi, H., Inagaki, E., Fujimoto, Y., Kuroishi, C., Nodake, Y., Nakamura, Y., Arisaka, F., Yutani, K., Kuramitsu, S., Yokoyama, S., Yamamoto, M., Miyano, M. & Tahirov, T. H. (2004). *Acta Cryst.* D**60**, 97–104.
Winn, M. D. *et al.* (2011). *Acta Cryst.* D**67**, 235–242.
Wu, C. A., Lokanath, N. K., Kim, D. Y., Park, H. J., Hwang, H.-Y., Kim, S. T., Suh, S. W. & Kim, K. K. (2005). *Acta Cryst.* D**61**, 1459–1464.
Wubben, T. J. & Mesecar, A. D. (2010). *J. Mol. Biol.* **404**, 202–219.
Yeates, T. O. (1988). *Acta Cryst.* A**44**, 142–144.
Yeates, T. O. (1997). *Methods Enzymol.* **276**, 344–358.